Creep and Rupture Properties of a Squeeze-Cast Mg-Al-Ca Alloy

S.M. ZHU, B.L. MORDIKE, and J.F. NIE

A squeeze-cast Mg-Al-Ca alloy (MRI153) was creep tested at 150, 175, and 200 °C under applied stresses in the range of 30 to 120 MPa. The creep curves were characterized by an extended tertiary stage in which the creep rate increases progressively with the creep strain. Microstructural examinations revealed the precipitation and coarsening of new particles during creep. The stress dependence of the minimum creep rate suggests a transition from power-law creep at low stresses to power-law breakdown at high stresses. Creep rupture of this alloy occurred as a result of cavitation damage at dendritic grain boundaries, with the creep rupture time and the minimum creep rate following the empirical Monkman-Grant equation. A comparison is made between the creep and rupture properties of MRI153 and those of a squeeze-cast Mg-Al alloy (AZ91).

I. INTRODUCTION

THERE are increasing demands from the automotive industry for low-cost magnesium casting alloys with sufficient strength and good creep resistance. Mg-Al–based alloys such as AZ91 (Mg-9Al-0.7Zn-0.2Mn; all compositions hereafter are in wt pct unless specified) and AM60 (Mg-6Al-0.3Mn) are the most commonly used magnesium alloys in automobiles because of a good combination of mechanical properties, corrosion resistance, and die castability. However, the use of Mg-Al alloys in automobiles has been restricted to components where creep resistance is of less concern, such as seat frames, steering wheels, instrument panels, valve covers, *etc*.[1] Since Mg-Al alloys exhibit inadequate creep resistance at temperatures above 125 °C, they are incapable of powertrain applications, where the operative temperatures can be as high as 175 °C for automatic transmission housings and 200 °C for engine blocks.[2]

MRI153, which was developed by Dead Sea Magnesium and Volkswagen AG for use as automatic transmission housings with complex geometries,[3] can be regarded as a modified version of AZ91. MRI153 contains Al (~9 pct) and Zn (~0.7 pct) to ensure its yield strength and castability, while Ca (~1 pct) and Sr (~0.1 pct) are added to form intermetallic phases at grain boundaries and in the grain interior to improve the creep resistance. It has been shown that MRI153 possesses superior properties such as yield strength, creep resistance, castability, and corrosion performance to AZ91.[3] For instance, the minimum creep rate of MRI153 at 135 °C under a load of 85 MPa is about one order of magnitude lower than that of AZ91. However, there is a lack of a more detailed study of the creep deformation process and rupture properties of this alloy.

Many studies have been conducted on the creep behavior of alloy AZ91 produced by various casting technologies, including die casting,[4–7] ingot casting,[8] squeeze casting,[9,10] and thixoforming.[11,12] The creep tests were generally conducted in the temperature range 120 to 200 °C, since the maximum operating temperature for AZ91 seldom or never exceeds 200 °C. In most studies,[4,5,6,8–12] stress exponents in the range 5 to 11 and activation energies close to that for self-diffusion in magnesium were obtained, suggesting a climb-controlled dislocation creep mechanism. However, Dargusch and Dunlop[7] reported stress exponents of 2 at low stresses and 5 at high stresses. They suggested that the low-stress creep behavior was related to grain boundary migration and sliding, which was accompanied by discontinuous precipitation of β-$Mg_{17}Al_{12}$ from the supersaturated α-Mg matrix. A recent review paper[13] compared the creep behavior of AZ91 alloys produced by different technologies. The difference in creep response was rationalized qualitatively by microstructural factors such as grain size and intragranular precipitates. A threshold stress that depends on the volume fraction and size of precipitate particles was introduced to describe the strengthening effect of intragranular precipitates. Skelenicka *et al*.[9,10] further investigated the strengthening effect of alumina fibers on the creep resistance of AZ91 and found that the reinforcement improved the creep resistance by a load-transfer effect without altering the dominant creep mechanism of the matrix.

The present paper describes a systematic study of the creep and rupture properties of a squeeze-cast MRI153 alloy. The temperature and stress dependence of creep rate is determined and the creep deformation mechanisms in the selected temperature and stress regime are analyzed. In addition, this paper presents long-time creep rupture data, which are expected to be of engineering value. Finally, the creep and rupture properties of MRI153 alloy are compared with those of a squeeze-cast AZ91 alloy, which allows for a more complete evaluation of the creep resistance of MRI153.

II. EXPERIMENTAL PROCEDURES

Blocks of MRI153 alloy, with dimensions of 60 × 100 × 100 mm, were produced by squeeze casting at the Technical University of Clausthal. Flat specimens with gauge dimensions of 3 × 6 × 27 mm were machined from the casting blocks for creep tests. No heat treatment was applied to the specimens prior to creep testing.

S.M. ZHU, Research Fellow, and J.F. NIE, Reader, are with the ARC Centre of Excellence for Design in Light Metals, Department of Materials Engineering, Monash University, Victoria 3800, Australia. Contact e-mail: suming.zhu@eng.monash.edu.au B.L. MORDIKE, Emeritus Professor, is with the Institute of Materials Engineering and Technology, Technical University of Clausthal, D-38678, Clausthal-Zellerfeld, Germany.

Manuscript submitted July 12, 2005.

Creep tests were performed in tension on constant-load creep machines at temperatures of 150, 175, and 200 °C and stresses ranging from 30 to 120 MPa. These temperatures were chosen because they are typical for the operation of automobile powertrain components. The creep specimens were heated by immersing in silicone oil baths. There are two advantages of using silicone oil as the heating medium: first, the temperature can be maintained very stable (within ±1 °C), and second, oxidation of specimens can be prevented. A rotating propeller ensured temperature uniformity in the baths. The creep strain was measured by extensometers attached directly to the gauge section of specimens and was recorded by a computer-controlled data acquisition system. To reduce the background noise caused by ambient temperature fluctuation, a reference extensometer was always used to compensate the strain readings. While most tests were run under constant load to the final failure of specimens, the tests at very low stresses were halted after the minimum creep rate was reached.

The microstructures of MRI153 before and after creep testing were examined using optical microscopy. Samples were mechanically ground with SiC papers, polished using silica suspension, and then etched in 1 pct Nital. The primary intermetallic particles were analyzed using an energy dispersive X-ray spectrometer (EDX) attached to a scanning electron microscope (SEM).

III. RESULTS

A. *Creep Tests*

The creep test conditions and resulting data for MRI153 are summarized in Table I. The parameters include test temperature (T), applied stress (σ), minimum creep rate ($\dot{\varepsilon}_m$), time to rupture (t_r), rupture strain (ε_r), and creep damage tolerance parameter (λ). The creep damage tolerance parameter represents the tolerance of a material to local strain concentration and is defined as:[14]

$$\lambda = \frac{\varepsilon_r}{\dot{\varepsilon}_m \cdot t_r} \qquad [1]$$

Similar creep curves were obtained for MRI153 at 150, 175, and 200 °C in the stress range of 30 to 120 MPa. Figure 1(a) shows the creep curves at four different stress levels at 175 °C. The creep strain rate, computed from the creep curves by differentiating the creep strain with respect to the creep time, is plotted against the creep strain in Figure 1(b). All of the creep curves exhibited a measurable instantaneous strain upon loading and a normal primary stage in which the creep rate decreased with increasing creep strain. However, a well-defined steady state was barely observed, especially at low stress levels. After a minimum value was reached, the creep rate increased progressively over the most creep duration. The progressive increase in creep rate over most of the creep duration is usually termed as "extended period of tertiary creep."[15] The extended tertiary creep became more pronounced at lower stresses for MRI153. For example, the extended tertiary creep started at a creep strain of ~4.0 pct for the stress level of 90 MPa, but it was evidenced at a creep strain of ~1.2 pct for the stress level of 60 MPa. There was a rapid increase in the creep rate in the late tertiary stage, which led to the final fracture of specimens.

Table I. Creep Test Conditions and Results for MRI153

T (°C)	σ (MPa)	$\dot{\varepsilon}_m(s^{-1})$	t_r (h)	ε_r (pct)	λ
150	120	2.9×10^{-6}	2.1	5.0	2.3
150	110	4.5×10^{-7}	19.3	5.6	1.8
150	100	1.2×10^{-7}	67.8	6.1	2.1
150	90	1.9×10^{-8}	488.5	5.4	1.6
150	80	5.7×10^{-9}	1570.5	5.7	1.8
150	70	2.0×10^{-9}	*	*	*
150	60	7.0×10^{-10}	*	*	*
175	110	8.9×10^{-6}	1.9	11.1	1.8
175	100	1.4×10^{-6}	10.5	10.2	1.9
175	90	5.0×10^{-7}	37.8	11.5	1.7
175	80	1.6×10^{-7}	100.5	9.7	1.7
175	70	3.9×10^{-8}	319.5	8.9	2.0
175	60	8.9×10^{-9}	986.8	6.3	2.0
175	50	2.5×10^{-9}	*	*	*
175	40	5.2×10^{-10}	*	*	*
200	90	6.8×10^{-6}	2.4	9.9	1.7
200	80	1.7×10^{-6}	10.5	9.7	1.5
200	70	3.2×10^{-7}	44.8	8.6	1.7
200	60	9.0×10^{-8}	134.4	8.1	1.9
200	55	4.9×10^{-8}	186.9	7.0	2.1
200	55	4.2×10^{-8}	208.8	6.9	2.2
200	50	2.2×10^{-8}	475.0	7.5	2.0
200	50	1.4×10^{-8}	670.8	7.8	2.3
200	40	3.4×10^{-9}	2007.8	8.4	3.4
200	30	5.4×10^{-10}	*	*	*

*These tests were interrupted after the minimum creep rate was reached.

B. *Microstructures Before and After Creep*

Optical micrographs of the initial microstructure of MRI153 in the squeeze-cast state are shown in Figure 2. Similar to that reported for die-cast AZ91,[6] the microstructure of MRI153 consisted of a primary α phase core surrounded by a solidified eutectic mantle (Figure 2(a)). Further examinations revealed that the eutectic was composed of coarse intermetallic particles embedded in α phase (Figure 2(b)). The eutectic α phase exhibited distinct contrast to the primary α phase, indicating that they had different solute concentrations. The eutectic particles can be classified into the following two types: type A particles had a lamellar appearance, while type B particles were irregularly shaped. These particles coexisted at the interdendritic boundaries. Another type of intermetallic particles (labeled as C in Figure 2) was observed occasionally and in minor quantity. Type C particles generally had a block shape and were distributed in a random manner. The compositions of these phases were analyzed semiquantitatively by EDX (Figure 3). The EDX results revealed that the eutectic α phase was saturated with Al. Type A particles, rich in Mg, Al, and Ca, were most likely $(Mg,Al)_2Ca$ compound, as observed in other Mg-Al-Ca alloys.[16,17,18] $(Mg,Al)_2Ca$ was reported to be a Laves phase with a crystal structure of C36 (hexagonal, a = 0.596 nm and c = 1.979 nm).[17,18] Detailed analysis of this phase is beyond the scope of this paper and will be reported elsewhere.[19] Type B particles were analyzed to be β-$Mg_{17}Al_{12}$ (bcc, a = 1.056 nm), with some Al atoms replaced by Zn atoms, since they had high concentrations of Mg and Al, and a small amount of Zn. The atomic ratio of Al and Mn in type C particles was very close to 8:5, so these particles were inferred to be Al_8Mn_5. The presence of β-$Mg_{17}Al_{12}$ and Al_8Mn_5

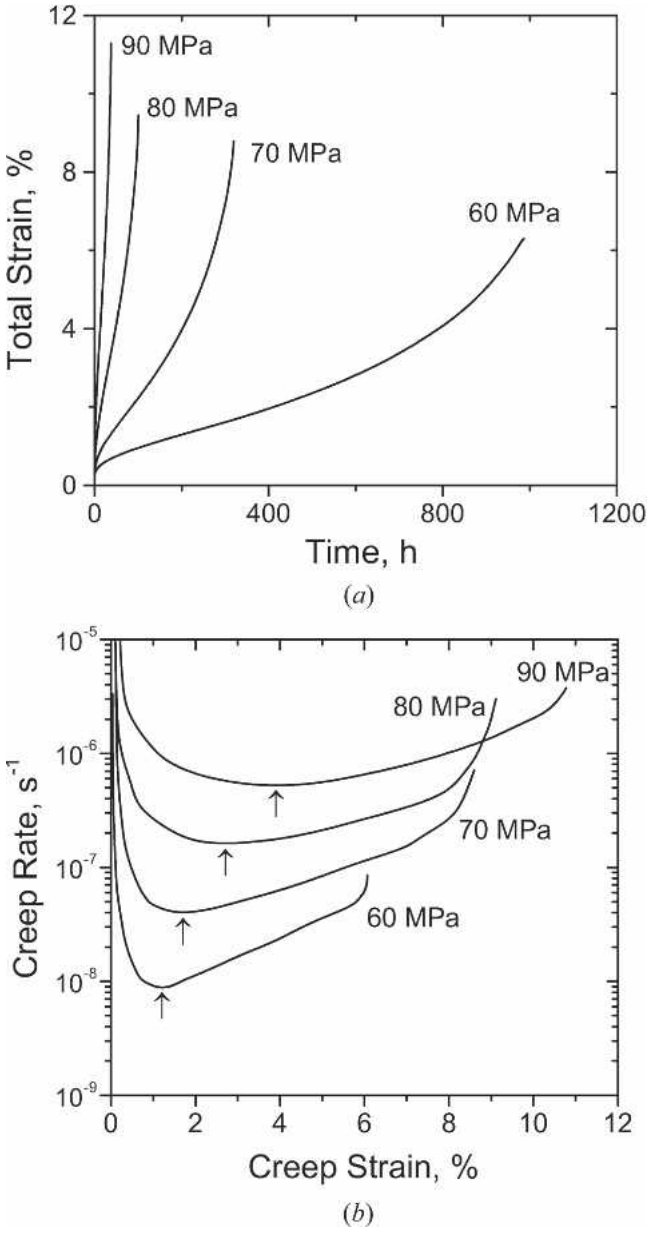

Fig. 1—Creep curves for MRI153 at 175 °C under various stresses: (*a*) total strain *vs* time and (*b*) creep rate *vs* creep strain. The arrows indicate where the minimum creep rate is reached.

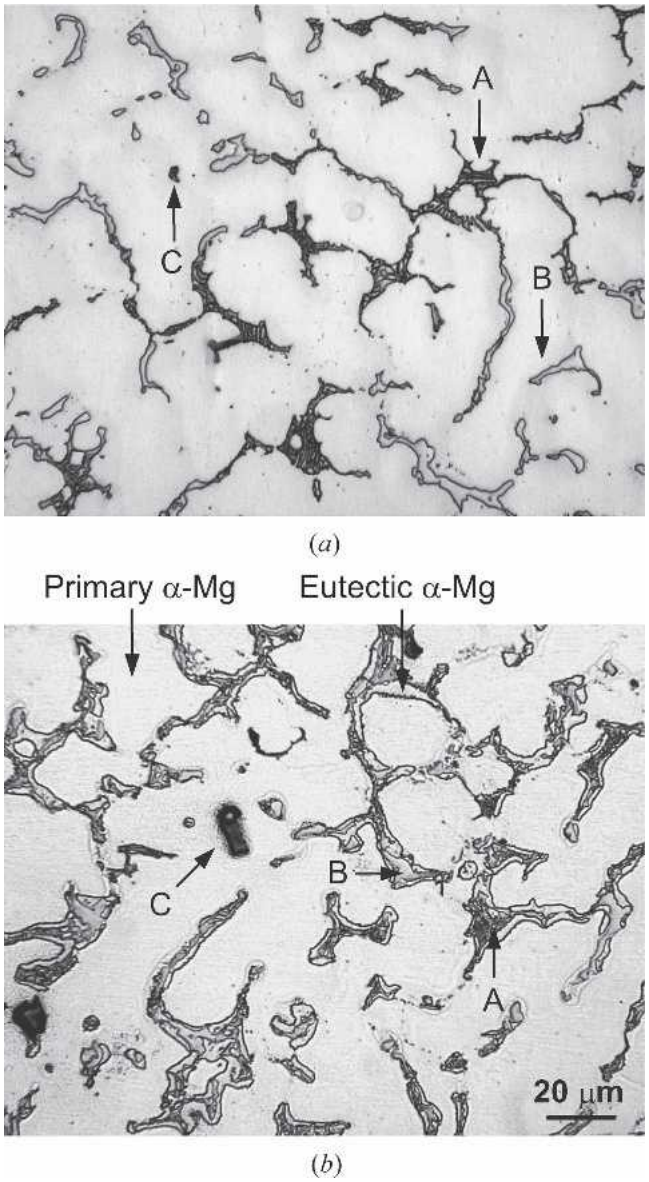

Fig. 2—Optical micrographs showing as-cast microstructure of MRI153: (*a*) sample lightly etched and (*b*) sample strongly etched in 1 pct Nital. Three different types of intermetallic particles are labeled as A, B, and C.

in MRI153 was not surprising, since these phases are common to as-cast AZ91.[20,21]

The microstructure of MRI153 underwent significant changes during creep. Figure 4 shows optical micrographs of creep specimens ruptured at different times. Besides the coarse eutectic particles already observed in the as-cast microstructure (Figure 2), new precipitate particles were seen in the ruptured specimens, and they tended to coarsen with increased testing time. Most of the precipitates were observed to form preferentially in the interdendritic regions where the supersaturated eutectic α solid solution resided. There was no evidence of any massive discontinuous precipitation as reported in die-cast AZ91 during creep.[7] These precipitates are considered to result from a dynamic precipitation process because dislocations introduced by creep deformation can act as sites for heterogeneous nucleation of precipitates. Sato *et al.*[22] reported similar precipitate particles in MRI153 after annealing at 200 °C for 48 hours. While most of the precipitate particles could be identified as β-$Mg_{17}Al_{12}$, the authors also observed another type of precipitate, probably $Mg_{21}(Zn,Al)_{17}$.

C. *Analysis of Minimum Creep Rate*

The minimum creep rate was correlated to the applied stress and temperature by the conventional power equation of the form

$$\dot{\varepsilon}_m = A\sigma^n \exp(-Q_c/RT) \qquad [2]$$

where A = a material-dependent constant, σ = the applied stress, n = the stress exponent, Q_c = the activation energy for creep, R = the gas constant, and T = the absolute temperature. Plots of the minimum creep rate against applied stress using logarithmic coordinates for MRI153 at temperatures

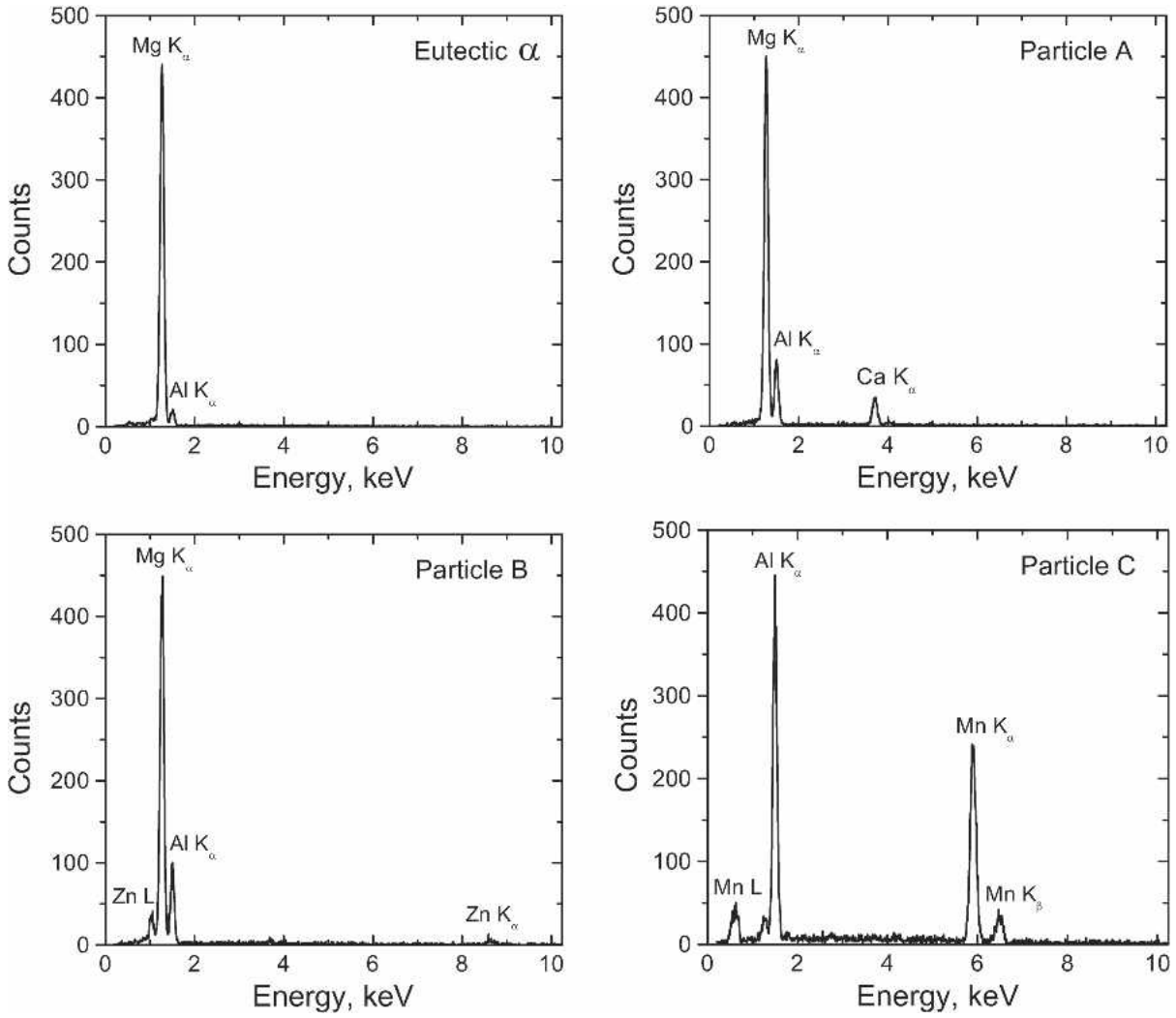

Fig. 3—EDX spectra of eutectic α-phase and intermetallic particles labeled in Figure 2.

of 150 to 200 °C are depicted in Figure 5. The stress exponent (*i.e.*, the slope of the plots) varied in the applied stress range, increasing from ~6 at low stresses to ~15 at high stresses. The stress dependence of the minimum creep rate was not altered by temperature change.

Arrhenius plots of the logarithm of minimum creep rate against the reciprocal of temperature at four stress levels are presented in Figure 6. The apparent activation energy for creep was determined from the slope. The plots yielded an activation energy value of ~165 kJ/mol at low stresses (60 and 70 MPa), which is higher than the activation energy for lattice self-diffusion in magnesium, 135 kJ/mol.[23] A much higher activation energy value of ~195 kJ/mol was obtained at high stresses (80 and 90 MPa).

D. *Creep Rupture Properties*

Creep rupture properties such as rupture time and rupture strain of MRI153 at three temperatures are shown in Figures 7(a) and (b), respectively. The rupture strain provides a direct measurement of the creep ductility of the alloy. The rupture time decreased with increasing test temperature or applied stress. No clear trend was apparent in the rupture strain with respect to changing rupture time at the three temperatures, except that the rupture strains at 175 and 200 °C were higher than those at 150 °C.

The relationship between the rupture time and the minimum creep rate is often described by the empirical Monkman–Grant equation:[24]

$$t_r \cdot \dot{\varepsilon}_m = C \qquad [3]$$

where C = a material-dependent constant. This relationship holds for most structural materials in which creep rupture is fully controlled by creep deformation. Figure 8 shows the correlation between the rupture time and the minimum creep rate using logarithmic coordinates. All the data fell on a single line with a slope of -1, indicating that creep rupture of MRI153 follows the Monkman–Grant relationship.

As shown in Table I, the values of λ were larger than 1 but less than 2.5 for most test conditions. According to Ashby and Dyson,[14] materials with λ values between 1 and 2.5 have low tolerance to strain concentration and would fail predominantly by intergranular cavitation. To study the accu-

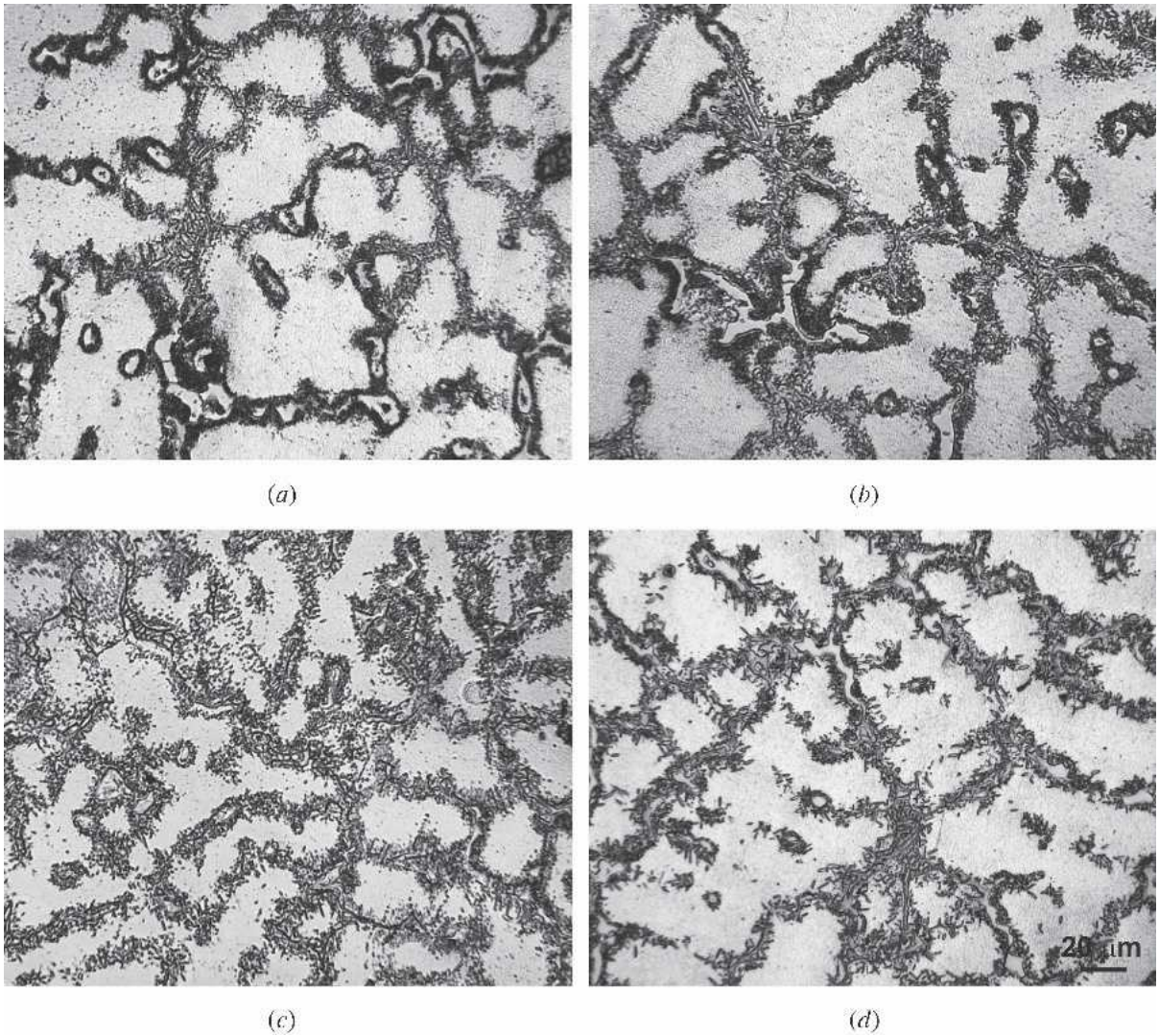

Fig. 4—Optical micrographs showing microstructures of creep specimens ruptured under different stresses at 200 °C: (*a*) 80 MPa (t_r = 10.5 hours), (*b*) 70 MPa (t_r = 44.8 hours), (*c*) 50 MPa (t_r = 475.0 hours), and (*d*) 40 MPa (t_r = 2007.8 hours). The samples were etched in 1 pct Nital.

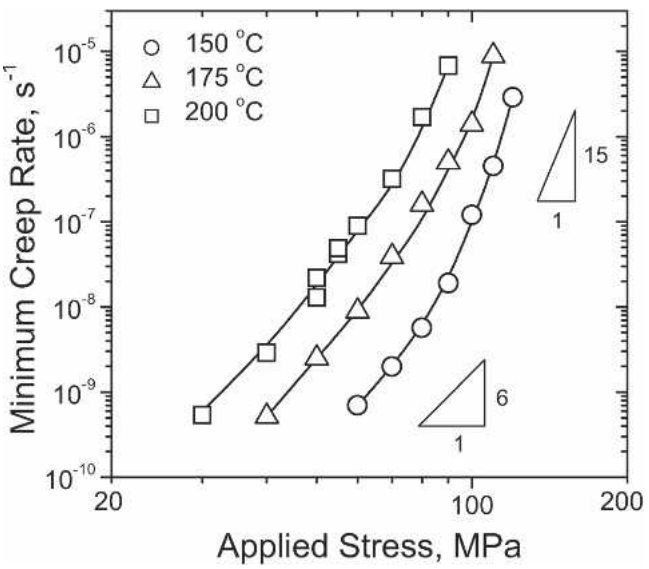

Fig. 5—Stress dependence of the minimum creep rate at 150, 175, and 200 °C.

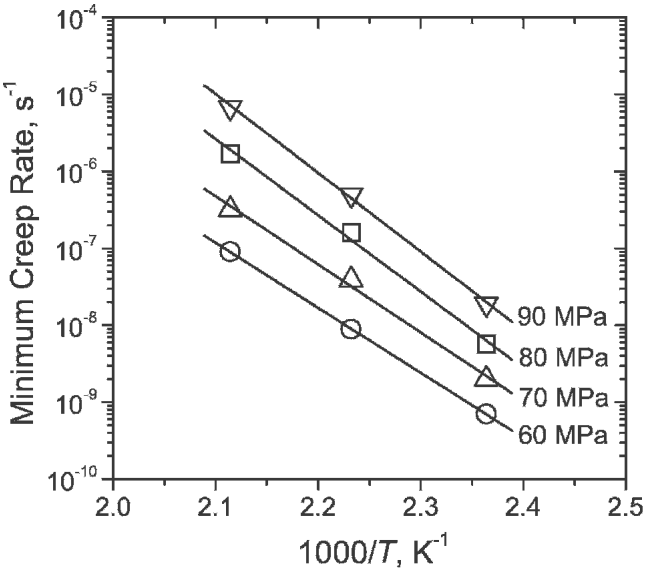

Fig. 6—Temperature dependence of the minimum creep rate for stress levels from 60 to 90 MPa.

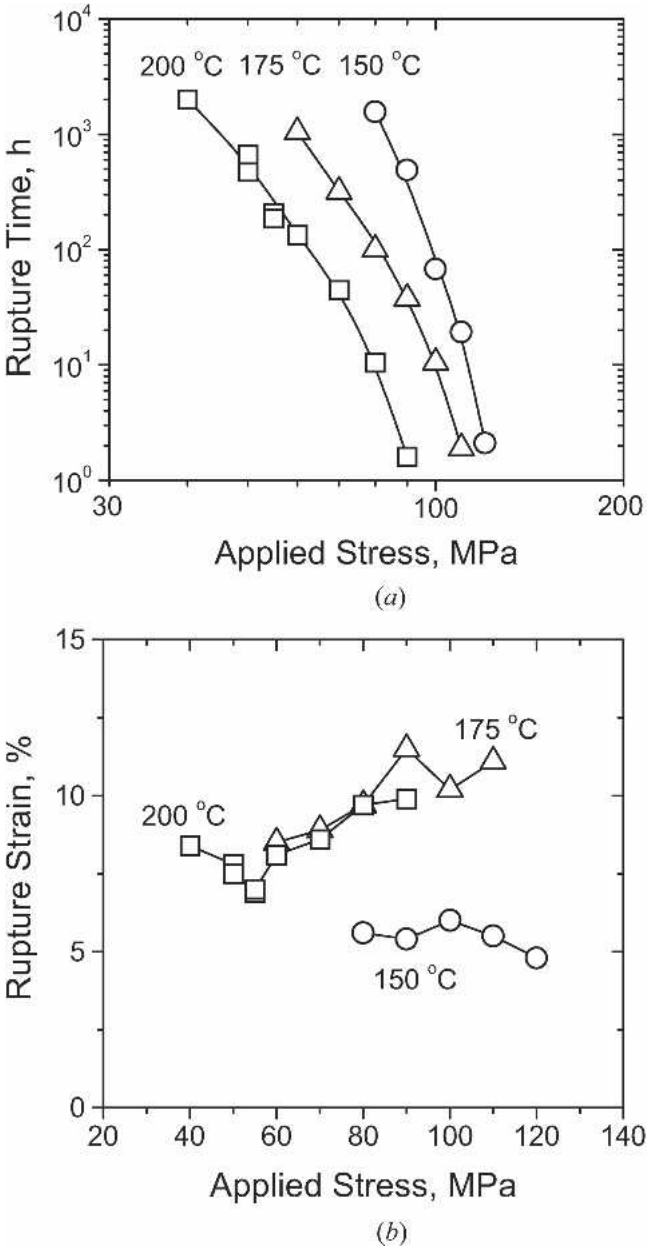

Fig. 7—Creep rupture properties at 150 and 200 °C: (*a*) rupture time *vs* applied stress and (*b*) rupture strain *vs* applied stress.

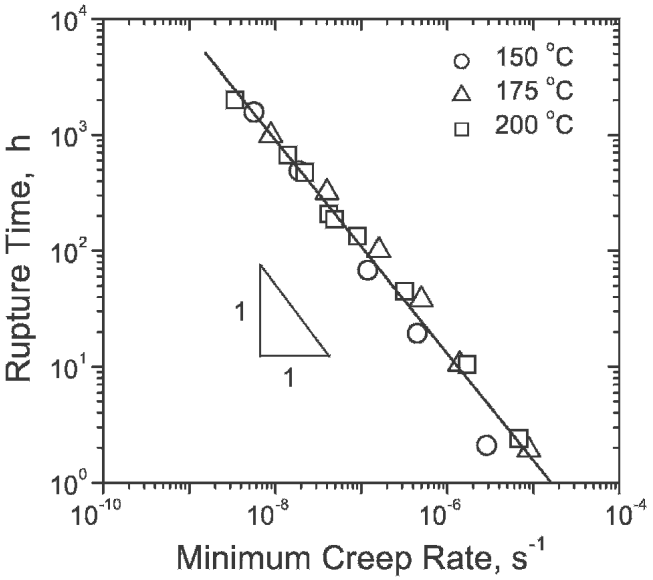

Fig. 8—Correlation of creep rupture time with the minimum creep rate.

mulated creep damage, the fractured specimens of MRI153 were sectioned and observed by optical microscopy. Figure 9 shows the longitudinal sections near the fracture surface of the specimens. Creep cavitation occurred mainly at dendritic grain boundaries of the primary α phase, where the eutectic particles resided. The growth and coalescence of the cavities led to the final fracture of the creep specimens.

IV. DISCUSSION

A. *Extended Tertiary Creep*

The most significant feature of the creep curves of MRI153 is the presence of the extended tertiary creep stage that dominates the overall creep process. Such extended tertiary creep has been observed in many engineering materials, such as Ni-based superalloys[25,26] and low alloy ferritic steels.[27,28] Contrary to conventional tertiary creep that arises from the loss of section by either external damage such as necking or internal damage in the form of creep cavitation, extended tertiary creep is usually associated with microstructural degradation.[14] The degradation of microstructure can take the following two forms: one is the coarsening and/or the dissolution of precipitate particles; the other is the strain softening due to an increase in the density or velocity of mobile dislocations. Recently Zhang *et al.*[29] reported observation of an extended tertiary stage in compressive creep of a die-cast AZ91 alloy and its associated microstructural changes. They concluded that the pronounced softening in the tertiary stage is related to the coarsening of secondary β-$Mg_{17}Al_{12}$ precipitates. In view of the significant microstructural changes that occurred during creep in this study, especially at low stresses, the observed extended tertiary creep in MRI153 is considered as associated with the coarsening of the precipitates that formed during the creep process.

B. *Possible Creep Mechanisms*

Studies[30,31] have been performed on the creep deformation behavior of dilute Mg-Al solid solution alloys over a wide range of temperatures and stresses. The main conclusions are summarized here. In a low temperature range, typically up to 300 °C, two deformation mechanisms may be operative, depending upon the stress level. At lower stresses, the Mg-Al alloys exhibit creep features that are typical for class I (alloy type) creep—*i.e.*, a very small instantaneous strain, a very brief primary creep stage, a stress exponent of ~3, an activation energy close to the activation energy for the diffusion of Al, and a concentration exponent of unity. It is well known that class I creep is controlled by the viscous glide of dislocations dragging solute atmospheres. However, at higher stresses, the stress exponent increases from ~3 to ~6. In addition, there is a measurable instantaneous strain and a well-defined primary stage in the creep curves.

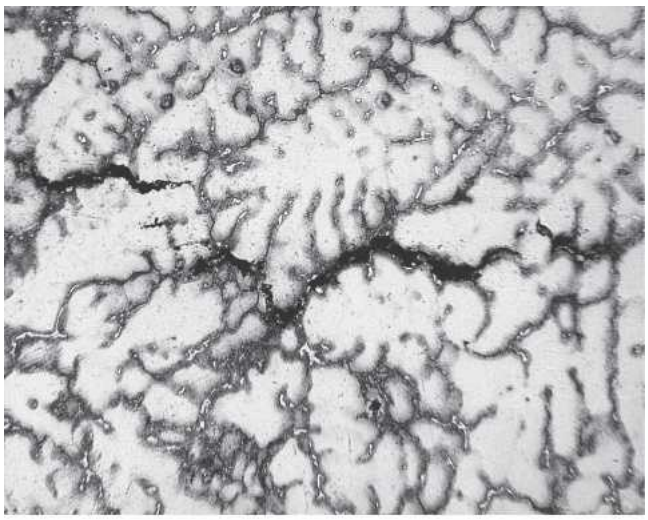

(*a*)

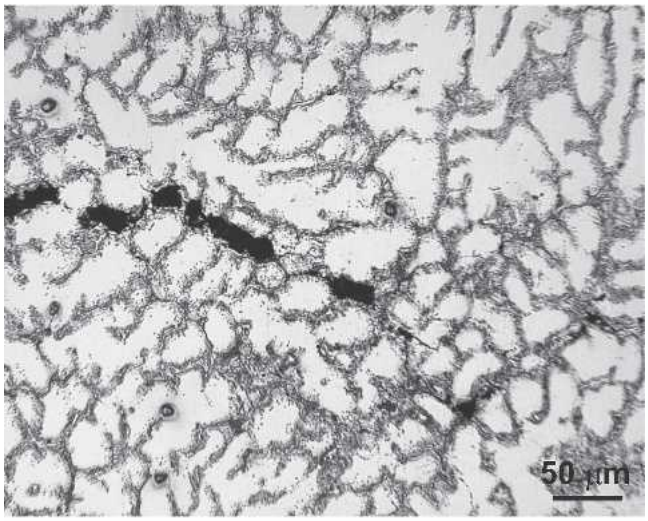

(*b*)

Fig. 9—Optical micrographs showing longitudinal section near the fracture surface of creep specimens: (*a*) 150 °C, 90 MPa and (*b*) 200 °C, 50 MPa. The stress direction is nearly vertical. The samples were etched in 1 pct Nital.

Dislocation climb is considered as the controlling creep mechanism at the higher stresses when the dislocations break away from their solute atmospheres. In a high temperature range, typically above 300 °C, creep deformation is characterized by a measurable instantaneous strain, a normal primary creep stage, a stress exponent of ~4, and an activation energy that decreases with increasing stress. The high-temperature creep behavior of the Mg-Al alloys is consistent with cross-slip of dislocations from the basal to the prismatic planes.

Since the creep tests conducted in this study revealed measurable instantaneous strains upon loading, a well-defined primary stage, and a stress exponent of ~6 at low stresses, it is reasonable to assume that the creep of MRI153 might be controlled by dislocation climb, which is usually related to lattice self-diffusion in magnesium. To verify this, the minimum creep rate normalized by the activation energy for

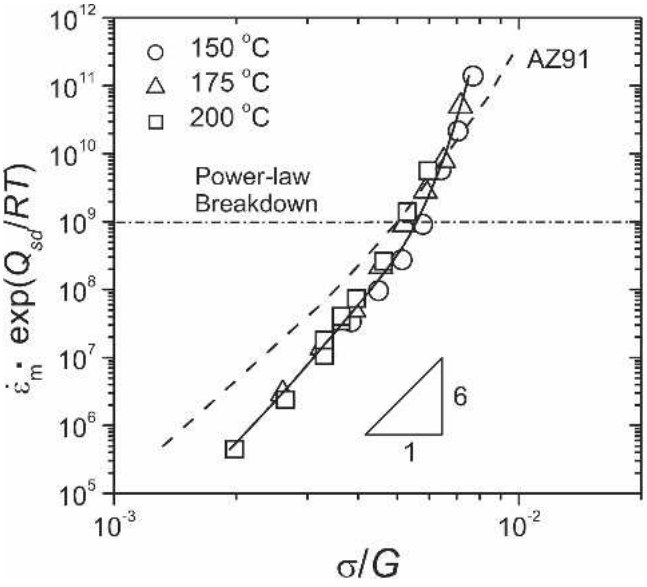

Fig. 10—Plot of the minimum creep rate normalized by activation energy for self-diffusion of magnesium (Q_{sd} = 135 kJ/mol) against stress normalized by shear modulus. Data for a squeeze-cast AZ91 alloy[9,10] are shown for comparison. Also shown is the Sherby-Burke criterion[33] for power-law breakdown.

lattice self-diffusion in magnesium is plotted against stress normalized by shear modulus in Figure 10. Here, the shear modulus for pure magnesium is used for the normalization, which is given as:[32]

$$G = (1.92 \times 10^4 - 8.6\,T)\ \text{MPa} \qquad [4]$$

It can be seen that the data at different temperatures merge well into a single master line, with a slope of ~6 at low stresses. This indicates that the lattice diffusion-controlled dislocation climb is most likely the operative creep deformation mechanism.

Also shown in Figure 10 is the criterion proposed by Sherby and Burke[33] for the power-law breakdown in creep of materials. According to this criterion, the power-law breakdown generally occurs when

$$\frac{\dot{\varepsilon}_m}{D} \approx 10^{13}\,\text{m}^{-2} \qquad [5]$$

where D = the lattice diffusion coefficient of the rate-controlling species. For the present alloy, D is put equal to the value for lattice self-diffusion in magnesium—*i.e.*, $D = 10^{-4}\exp(-Q_{sd}/RT)\ \text{m}^2\ \text{s}^{-1}$, where Q_{sd} is the activation energy for lattice self-diffusion in magnesium. From this figure, the power-law breakdown behavior of MRI153 appears to comply with the Sherby–Burke criterion. Thus, the stress exponent increase with increasing stress can be attributed to the transition from power-law creep at low stresses to power-law breakdown at high stresses.

The higher activation energy value obtained for MRI153 at high stresses (~195 kJ/mol) than that at low stresses (~165 kJ/mol) might be related to the breakdown of power-law creep, as reported for an Al-10Zn alloy.[34] However, even the activation energy value at low stresses is still higher than that for lattice self-diffusion in magnesium. According to the

literature,[35] materials with a dispersion of second-phase particles, especially at grain boundaries, usually exhibit creep activation energies that are higher than those for lattice self-diffusion of the matrix, provided that these particles are sufficiently stable and can act as effective obstacles to dislocation movement. The relatively high activation energy obtained at low stresses for MRI153 is considered to be associated with the eutectic $(Mg,Al)_2Ca$ intermetallic phase at grain boundaries. $(Mg,Al)_2Ca$ is reported to be more stable than β-$Mg_{17}Al_{12}$ at high temperatures.[17] The presence of $(Mg,Al)_2Ca$ particles may provide obstacles to dislocation movement by inhibiting the annihilation process of dislocations at grain boundaries, thus increasing the dislocation density near grain boundaries. The eutectic $(Mg,Al)_2Ca$ phase also accounts for the superior creep resistance of MRI153 to AZ91, as discussed in the following section.

C. *Comparison with Squeeze-Cast AZ91*

Since MRI153 has been developed as a potential substitute to AZ91 for applications that require higher creep resistance, the creep properties must be compared to those of AZ91. There are many open publications on the creep properties of AZ91; however, materials produced by different processing technologies tend to exhibit quite different creep properties, owing to changes in microstructural features such as volume fraction and distribution of β-$Mg_{17}Al_{12}$ phase, grain size of primary α phase, and Al content in solid solution.[13] To avoid the influence of processing technologies, creep properties of a squeeze-cast AZ91[9,10] were used for comparison in the current study.

The temperature-normalized minimum creep rate as a function of the normalized stress for the squeeze-cast AZ91 is depicted in Figure 10 to compare with data obtained for MRI153. The following two points can be deduced from the comparison. First, the two alloys show similar creep deformation behavior: power-law creep at low stresses and power-law breakdown at high stresses. The stress exponents are ~5 for AZ91 and ~6 for MRI153 in the power-law regime, which are indicative of dislocation climb controlled creep deformation. Second, MRI153 exhibits much better creep resistance than AZ91 in terms of the minimum creep rate in the power-law regime. However, at very high stresses (power-law breakdown regime), the creep resistance of MRI153 is poorer than that of AZ91. This point is also apparent from the comparison of the rupture times of the two alloys at 150 and 200 °C (Figure 11). MRI153 has longer rupture times at low stresses but shorter rupture times at high stresses compared to AZ91.

The creep resistance of Mg-Al base alloys depends on the solid solution strengthening of Al, precipitation strengthening by β-$Mg_{17}Al_{12}$ within grains, and grain boundary strengthening by eutectic β-$Mg_{17}Al_{12}$. The eutectic β-$Mg_{17}Al_{12}$ contributes to the creep resistance by obstructing the dislocation annihilation (recovery) in dislocation creep or inhibiting grain boundary migration and/or grain boundary sliding in diffusional creep. However, due to its low melting point, β-$Mg_{17}Al_{12}$ tends to coarsen at elevated temperatures, thus losing its strengthening effect. Therefore, the creep resistance of Mg-Al alloys would be improved if β-$Mg_{17}Al_{12}$ is fully replaced or partially inhibited by another intermetallic phase with relatively higher thermal stability. Several studies have shown improved creep resistance of Mg-Al alloys by adding Ca.[16,36,37,38] Some researchers[36,37] explained the improved creep resistance by the formation of a more stable Al_2Ca and the suppression of β-$Mg_{17}Al_{12}$. Terada *et al.*[38] reported the beneficial effect of Ca on creep resistance of AM60, without identifying the eutectic phases. Luo *et al.*[16] ascribed the improved creep resistance in Mg-5Al-3Ca alloys to the inhibition of grain boundary sliding inhibition by $(Mg,Al)_2Ca$, especially at low stresses. In the current study, the better creep resistance exhibited by MRI153 than AZ91 in the power-law creep regime is attributed to the presence of eutectic $(Mg,Al)_2Ca$ phase at grain boundaries. Since grain boundary sliding is not the rate-controlling creep mechanism in the power-law regime, $(Mg,Al)_2Ca$ is considered to improve creep resistance by obstructing the dislocation annihilation at grain boundaries.

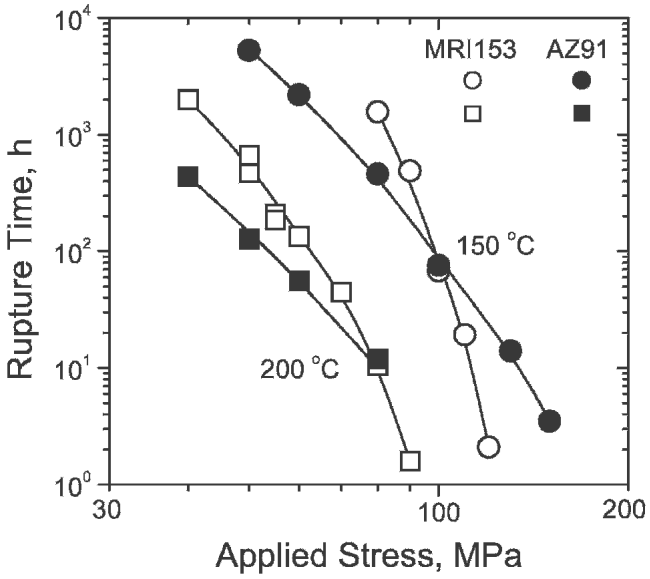

Fig. 11—Comparison the creep rupture times of MRI153 and a squeeze-cast AZ91 alloy[9,10] at 150 and 200 °C.

Finally, we will discuss why MRI153 exhibits poorer creep resistance than AZ91 in the power-law breakdown regime. In the power-law breakdown regime, creep deformation is controlled by glide-controlled flow, a process similar to low-temperature yield behavior. One factor for consideration is the yield strength. MRI153 was tested in the as-cast condition without any heat treatments, while AZ91 was given a T6 heat treatment (solution-treated at 415 °C for 24 hours, air cooled, and then aged at 170 °C for 24 hours),[9,10] which probably led to a peak hardening in AZ91. A yield strength ($\sigma_{0.2}$) of 93 MPa was obtained for the present MRI153 at 150 °C, which is apparently lower than that reported for AZ91 (105 MPa).[3] Although the yield strength of the squeeze-cast AZ91 in references 9 and 10 is not available, it is reasonable to assume that the squeeze-cast AZ91 has higher yield strength than the present MRI153. Consequently, AZ91 exhibited lower creep rates and longer rupture times than the MRI153 in creep at high stresses. Another factor we may consider is the work hardening rate. Blum *et al.*[39] attributed the better creep resistance observed in die-cast AZ91 than in die-cast AS21, AS41, and AE42 at high stresses to high rate of work hardening, which is related to the high initial content of Al solute. MRI153 is expected to have a

lower content of Al solute than AZ91 because the Ca addition may lower the solid solubility of Al in the magnesium matrix. Further work, especially creep tests on heat-treated specimens, is needed to exclusively explain this difference in creep resistance.

V. CONCLUSIONS

The creep and rupture properties of squeeze-cast MRI153 have been studied in the temperature range 150 to 200 °C at stresses from 30 to 120 MPa. The following conclusions are drawn:

1. The creep curves of MRI153 are dominated by an extended tertiary stage, which is associated with the precipitation and coarsening of new particles during the creep process.
2. The stress exponent of the minimum creep rate increases from ~6 at low stresses to ~15 at high stresses, indicating a transition in creep deformation behavior from power-law creep to power-law breakdown with increasing stress.
3. Creep cavitation occurs mainly at the dendritic grain boundaries for MRI153. The relationship between creep rupture time and the minimum creep rate of MRI153 can be well described by the empirical Monkman–Grant equation.
4. Compared with the squeeze-cast AZ91, MRI153 exhibits significantly higher creep resistance in the power-law creep regime. The improved creep resistance is attributed to the formation of eutectic $(Mg,Al)_2Ca$ phase.

ACKNOWLEDGMENT

Financial support by the Australian Research Council (ARC) is gratefully acknowledged.

REFERENCES

1. I.A. Anyanwu, Y. Gokan, S. Nozawa, A. Suzuki, S. Kamado, Y. Kojima, S. Takeda, and T. Ishida: *Mater. Trans*., 2003, vol. 44, pp. 562-70.
2. A.A. Luo: in *Magnesium Technology 2000*, H.I. Kaplan, J. Hryn, and B. Clow, eds., TMS, Warrendale, PA, 2000, pp. 89-98.
3. F. von Buch, S. Schumann, H. Friedrich, E. Aghion, B. Bronfin, B.L. Mordike, M. Bamberger, and D. Eliezer: in *Magnesium Technology 2002*, H.I. Kaplan, ed., TMS, Warrendale, PA, 2002, pp. 61-67.
4. W. Blum, P. Weidinger, B. Watzinger, R. Sedlacek, R. Rosch, and H.G. Haldenwanger: *Z. Metallkd*, 1997, vol. 88, pp. 636-41.
5. M. Regev, E. Aghion, M. Bamberger, and A. Rosen: *Mater. Sci. Eng.*, 1997, vol. A234–236, pp. 123-26.
6. W. Blum, B. Watzinger, and P. Zhang: *Adv. Eng. Mater*., 2000, vol. 2, pp. 349-55.
7. M.S. Dargusch and G.L. Dunlop: in *Magnesium Alloys and Their Applications*, B.L. Mordike and K.U. Kainer, eds., Werkstoff-Informationsgesellschaft, Frankfurt, Germany, 1998, pp. 277-82.
8. M. Regev, E. Aghion, A. Rosen, and M. Bamberger: *Mater. Sci. Eng*., 1998, vol. A252, pp. 6-16.
9. V. Skelenička, M. Pahutová, K. Kuchařová, M. Svoboda, and T.G. Langdon: *Metall. Mater. Trans*., 2002, vol. 33A, pp. 883-89.
10. M. Svoboda, M. Pahutová, K. Kuchařová, V. Skelenička, and T.G. Langdon: *Mater. Sci. Eng*., 2002, vol. A324, pp. 151-56.
11. S. Spigarelli: *Scripta Mater*., 2000, vol. 42, pp. 397-402.
12. S. Spigarelli, M. Cabibbo, E. Evangelista, M. Talianker, and V. Ezersky: *Mater. Sci. Eng.*, 2000, vol. A289, pp. 172-81.
13. S. Spigarelli, M. Regev, E. Evangelista, and A. Rosen: *Mater. Sci. Technol*., 2001, vol. 17, pp. 627-38.
14. M.F. Ashby and B.F. Dyson: in *Advances in Fracture Research*, S.R. Valluri, D.M.R. Taplin, P. Rama Rao, J.F. Knott, and R. Dubcy, eds., Pergamon Press, Oxford, U.K., 1984, vol. 1, pp. 3-30.
15. B.F. Dyson and T.B. Gibbons: *Acta Metall*., 1987, vol. 35, pp. 2355-69.
16. A.A. Luo, M.P. Balogh, and B.R. Powell: *Metall. Mater. Trans*., 2002, vol. 33A, pp. 567-74.
17. A. Suzuki, N.D. Saddock, J.W. Jones, and T.M. Pollock: *Scripta Mater*., 2004, vol. 51, pp. 1005-10.
18. A. Suzuki, N.D. Saddock, J.W. Jones, and T.M. Pollock: *Acta Mater*., 2005, vol. 53, pp. 2823-34.
19. S.M. Zhu and J.F. Nie: unpublished research.
20. E. Aghion and B. Bronfin: in *Proceedings of 3rd International Magnesium Conference*, G.W. Lorimer, ed., Institute of Materials, London, U.K., 1997, pp. 313-25.
21. J. Kiehn, K.U. Kainer, P. Vostrý, and I. Stulíková: *Phys. Stat. Sol*., 1997, vol. 161, pp. 85-95.
22. T. Sato, B.L. Mordike, J.F. Nie, and M.V. Kral: in *Magnesium Technology 2005*, N.R. Neelameggham, H.I. Kaplan, and B.R. Powell, eds., TMS, Warrendale, PA, 2005, pp. 435-40.
23. H.J. Frost and M.F. Ashby: *Deformation Mechanism Maps*, Pergamon Press, Oxford, U.K., 1982, p. 328.
24. F.C. Monkman and N.J. Grant: *Proc. ASTM*, 1956, pp. 593-620.
25. H. Burt, J.P. Denison, and B. Whishire: *Metal. Sci*., 1979, vol. 13, pp. 295-301.
26. R.A. Stevens and P.E.J. Flewitt: *Acta Metall*., 1981, vol. 29, pp. 867-82.
27. F. Abe, S. Nakazawa, H. Araki, and T. Noda: *Metall. Trans*, 1992, vol. 23A, pp. 469-77.
28. B.K. Choudhary, K. Saroja, K. Bhanu Sankara Rao, and S.L. Mannan: *Metall. Mater. Trans*., 1999, vol. 30A, pp. 2825-34.
29. P. Zhang, B. Watzinger, and W. Blum: *Phys. Stat. Sol*., 1999, vol. 175, pp. 481-89.
30. S.S. Vagarali and T.G. Langdon: *Acta Metall*., 1982, vol. 30, pp. 1157-70.
31. K. Maruyama, M. Suzuki, and H. Sato: *Metall. Mater. Trans*., 2002, vol. 33A, pp. 875-82.
32. S.S. Vagarali and T.G. Langdon: *Acta Metall*., 1981, vol. 29, pp. 1969-82.
33. O.D. Sherby and P.M. Burke: *Prog. Mater. Sci*., 1967, vol. 13, pp. 325-90.
34. M.S. Soliman: *J. Mater. Sci*., 1987, vol. 22, pp. 3529-32.
35. J. Čadek: *Creep in Metallic Materials*, Elsevier, Amsterdam, The Netherlands, 1988, p. 176.
36. H. Gjestland, G. Nussbaum, and G. Regazzoni: *Mater. Sci. Eng*, 1991, vol. A134, pp. 1197-200.
37. M.O. Pekguleryuz and J. Renaud: in *Magnesium Technology 2000*, H.I. Kaplan, J. Hryn, and B. Clow, eds., TMS, Warrendale, PA, 2000, pp. 279-84.
38. Y. Terada, R. Sota, N. Ishimatsu, T. Sato, and K. Ohori: *Metall. Mater. Trans*., 2004, vol. 35A, pp. 3029-32.
39. W. Blum, P. Zhang, B. Watzinger, B. van Grossman, and H.G. Haldenwanger: *Mater. Sci. Eng*, 2001, vol. A319–321, pp. 735-40.